Influence of UV irradiation and ozone on atmospheric corrosion of bare silver

Z. Y. Chen[1], D. Liang[2], G. Ma[3], G. S. Frankel[2], H. C. Allen[3] and R. G. Kelly*[1]

The corrosion of Ag in an atmosphere of ozone and humidity with or without irradiation by ultraviolet (UV) light was investigated. A modified coulometric reduction technique was used, substituting sulphate solution for chloride solution, to prevent the spontaneous transformation of silver oxide corrosion product to chloride in the reduction solution. The presence of both ozone and UV radiation was required for fast corrosion of Ag to occur. The amount of corrosion product for a given exposure time increased with ozone concentration, whereas the relative humidity had little effect. An incubation time for the corrosion reaction was observed. The presence of both ozone and UV radiation were necessary for rapid corrosion because the photodissociation of ozone generates reactive atomic oxygen, which reacts with Ag rapidly to form Ag_2O. The corrosion reaction on bare silver was minimally affected by the relative humidity in the environment, which is contrary to common atmospheric corrosion experience.

Keywords: Atmospheric corrosion, Silver, Ozone, Photoinduced corrosion

Introduction

The susceptibility of materials to atmospheric corrosion is often assessed by exposure to accelerated exposure testing such as the salt spray environment described by ASTM B117.[1] However, the correspondence between assessments made from lab and field exposures is generally poor. For example, silver is usually heavily corroded in field exposures at coastal sites but is barely attacked during exposure in a salt spray chamber environment.

Recent studies in atmospheric chemistry have revealed that interactions among UV light, chloride aerosols[2–4] and oxidising agents such as ozone[2,5–7] create reactive species such as atomic oxygen, hydroxyl radical, $HOCl^-$ as well as atomic and molecular chlorine. It is possible that these species can be transported long distances in the atmosphere to locations far from oceans[8] and have effects on the atmospheric corrosion of metals.

Atmospheric corrosion of silver is affected by many factors, and relative humidity (RH) is a factor that is well known to play an important role as atmospheric corrosion generally increases with increasing RH. Atmospheric corrosion of silver was observed only in the presence of moisture, and the amount of moisture adsorbed on silver surface was a function of RH.[9–11] However, Rice *et al.*[12] observed that the atmospheric corrosion rate of silver was insensitive to RH over the range of 30–80% in lab chamber environments consisting of purified humid air containing predetermined quantities of SO_2, NO_2, H_2S, Cl_2, HCl, NH_3 and O_3. This lack of RH dependence was attributed to direct chemical attack of Ag by H_2S. The deposition of airborne environmental pollutant particles on the surface also plays an important factor in the atmospheric corrosion of silver.[13–15] Air flow conditions, gravity, electrostatic forces and temperature gradients strongly influence the atmospheric corrosion rate through their influences on the transport of the airborne pollutants to the metal surface.[16,17] Silver is very sensitive to O_3, NH_3, H_2S and Cl_2[9–13,15,18,19] but relatively insensitive to HCl[12] and SO_2.[12,20] Oxidising species such as O_3, NO_2 and Cl_2 can also enhance the formation rate of Ag_2S. Common corrosion products are Ag_2S and AgCl.[12,14,21–24]

Although considerable research has been performed to simulate silver sulphidation with lab exposure, little work has been done on photo assisted corrosion of silver.[25] The wavelength of sunlight reaching the earth's atmosphere is from 100 to 10^6 nm.[26] Ultraviolet (UV) wavelengths shorter than 290 nm are absorbed by molecular oxygen, ozone and water vapour in the upper atmosphere, and hence, they do not reach the surface of the earth in measurable amounts. However, longer wavelength UV radiation does reach the earth and can affect the corrosion of metals exposed outdoors. Polarisation test results revealed that UV radiation can suppress the pitting generation rate[27,28] and enhance the passivity of SS304 in chloride solution.[29–32] In contrast, increasing corrosion rate from UV radiation was also observed.[33] The intensity of UV radiation seems to affect the corrosion properties of SS304 with improvement of corrosion properties at lower intensities and deterioration at higher intensities.[34,35] The effect of UV

[1]Department of Materials Science and Engineering, University of Virginia, Charlottesville, VA 22904, USA
[2]Department of Materials Science and Engineering, The Ohio State University, Columbus, OH 43210, USA
[3]Deptartment of Chemistry, The Ohio State University, Columbus, OH 43210, USA

*Corresponding author, email rgk6y@virginia.edu

Published by Maney on behalf of the Institute
Received 10 September 2009; accepted 16 November 2009
DOI 10.1179/147842209X12579401586681

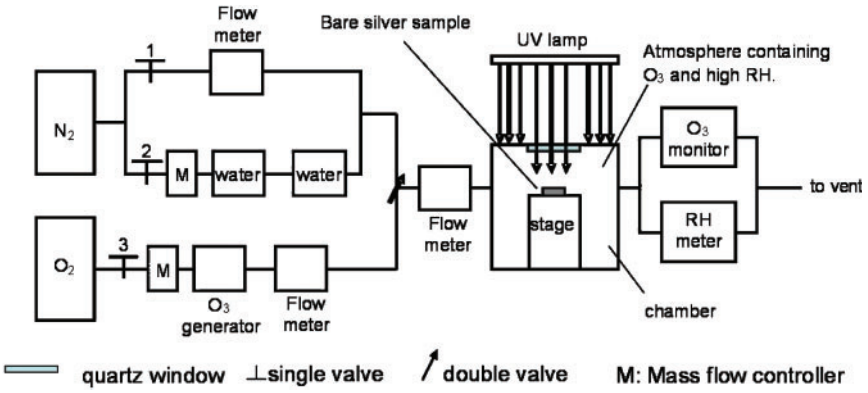

1 Schematic drawing of gas route and chamber

radiation is not limited to steels. Ultraviolet radiation enhanced the passivity on tin[36] and copper alloys.[37] However, negative UV radiation effects on the passivity of zinc alloys have also been documented.[38–40] Certainly, the semiconducting properties of oxide covered surfaces can be affected by radiation.

Ultraviolet light can also alter the environment, as it can decompose ozone to form atomic oxygen as shown in reaction (1).[5,41,42] If the wavelength is short enough, it can also split molecular oxygen to form two oxygen atoms as shown in reaction (2)[41]

$$O_3 \xrightarrow{h\nu(\lambda<310\text{nm})} O + O_2 \quad (1)$$

$$O_2 \xrightarrow{h\nu(\lambda<242\text{nm})} O + O \quad (2)$$

The goal of this work was to investigate the effects of UV radiation on the corrosion of silver under atmospheric conditions. There are key questions regarding the nature and concentration of the species that form in the atmosphere and their influence on the corrosion process. In this work, the effects of ozone, UV radiation and RH on the atmospheric corrosion behaviour of bare Ag (i.e., with no chloride particles deposited on the surface) were examined in an exposure chamber. The corrosion products were studied by coulometric reduction, scanning electron microscopy (SEM) and energy dispersive spectroscopy (EDS). Possible mechanisms for atmospheric corrosion by ozone and UV radiation are proposed. A subsequent paper will discuss the behaviour of silver with salt particles deposited on the surface.

Experimental

Silver samples of 99·9% purity were used in the experiments. Samples were $\sim 17 \times 17$ mm in size (2 mm thick) and were wet polished with SiC paper to 600 grit before being ultrasonically cleaned in analytical grade ethanol for 5 min. The samples were then put into a desiccator for 24 h before exposure.

Figure 1 is a schematic of the experimental apparatus that was used. Pure oxygen gas passed through an ozone generator (Jelight model 600) to generate the desired level of ozone and was then combined with a mixture of dry and water saturated pure N_2 gas to set the desired RH in the exposure chamber. In these experiments, a halocarbon wax coated acrylic chamber and a glass chamber were used separately. Although the details of gas flow might be different in these two chambers, the effect of chamber material on the corrosion rate of Ag is believed to be negligible, as both surfaces are inert to atomic oxygen. The RH was monitored with a Fisher Scientific Traceable RH meter. The concentration of ozone was controlled by varying the exposed length of the lamp inside the ozone generator and also by the mixing ratio with the N_2 gas. The flowrates of O_2 and N_2 were controlled by digital MKS Type 1179A O_2 and N_2 Mass-Flo controllers respectively. These controllers allowed an N_2 flow range of 20–1000 cm^3 min^{-1} and an O_2 flow range of either 0·5–10 or 10–500 cm^3 min^{-1}, depending on the particular O_2 Mass-Flo controller used. The primary source of UV light was a 254 nm UV lamp (UVP model XX-15S), which illuminated the sample inside the chamber through a UV transparent quartz window mounted in a polytetrafluoroethylene chamber cover. Even though the spectrum of sunlight is broad and mostly cuts off at 290 nm, the 254 nm UV light was used to accelerate the reactions with higher energy.[5,41,42] The UV lamp intensity was measured to be 4 mW cm^{-2} at a distance of 12·7 cm. The spectrum of the UV lamp used in the experiment was measured with an Ocean Optics USB2000 UV-vis at a distance of 18 cm. A strong peak was observed at around 254 nm, as well as at 311, 372, 402, 435, 545 and 578 nm. The chamber exit gas ozone concentration was measured by an Ozone Engineering model 465L ozone monitor, which can detect concentrations from 50 ppb to 50 ppm.

The effects of UV radiation, ozone and RH on the corrosion of bare Ag were investigated using the following exposure conditions:

(i) O_3 and RH environment with or without UV radiation (i.e., in the dark)
(ii) RH and UV radiation environment with and without O_3 (but with O_2)
(iii) UV radiation with O_3 environment at various RH ranging from 90 to 0%.

When the gas stream was not passed through the water flasks for hydration, the reading on the RH meter was zero. However, the meter is only valid for RH values to 10%, so 0% RH only represents a value of $<10\%$ RH. A fixed exposure time of 22 h was used for most experiments, but experiments were also performed to investigate the amount of corrosion product formed as a function of exposure time. Finally, a piece of silver was first exposed to an environment with both O_3 and UV radiation and then put into an ASTM B117 salt spray chamber for about 2 weeks.

Coulometric reduction was used to quantify the amount and identify the type of corrosion product on

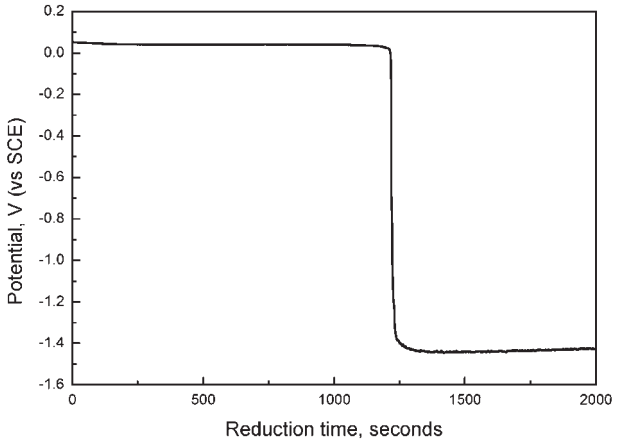

2 Typical coulometric reduction curve for silver chloride in deaerated 0·1M KCl. Silver chloride was formed at 2 mA cm^{-2} for 60 s in 0·1M KCl. Reduction current density was −0·1 mA cm^{-2}

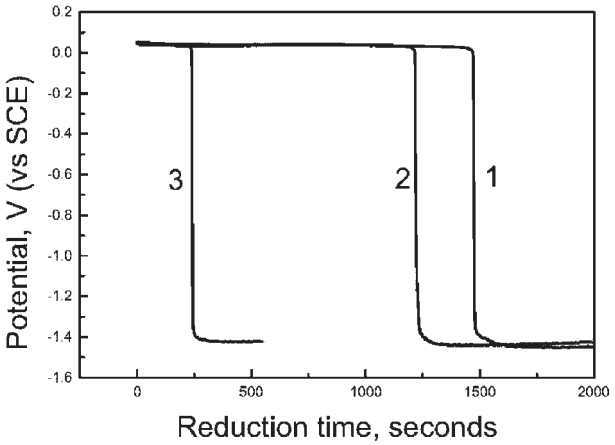

3 Potential versus time for coulometric reduction (−0·1 mA cm^{-2}) of oxidised silver samples in deaerated 0·1M KCl solution. Before reduction, silver chloride was formed by coulometric oxidation at 2 mA cm^{-2} for 60 s in 0·1M KCl solution and/or silver oxide was formed by potentiodynamic scan from −1680 to 900 mV with a rate of 100 mV s^{-1} in 1M NaOH solution. Curve 1 is the reduction of Ag sample with both silver oxide and silver chloride formed. Curve 2 is the reduction of Ag sample with only silver chloride formed. Curve 3 is the reduction of Ag sample with only silver oxide formed

the silver surface. Coulometric reduction was performed in a standard flat cell made of acrylic using a Gamry Reference 600 potentiostat. The silver electrode area was 1 cm^2. The electrolytes used were either 0·1M KCl or 0·1M Na_2SO_4 adjusted to pH 10 with NaOH. In all cases, the solutions were deaerated for at least 1 h before testing. The sample potential was measured during application of a constant cathodic current density that was usually −0·1 mA cm^{-2}. A saturated calomel electrode (SCE) was used in the chloride electrolyte, and a saturated Hg/Hg_2SO_4 electrode (MSE) was used in the sulphate electrolyte. The MSE potential was measured to be ∼381 mV higher than that of SCE, and the data are reported according to the electrode used in the particular experiments. The reduction curves exhibited potential plateaus that are distinctive for different corrosion products. The time period of each plateau, which is directly related to charge at a constant current, can be used to quantify the amount of each corrosion product.

Results

Coulometric reduction technique

Figure 2 shows a typical coulometric reduction curve. This sample was first treated by passing an anodic current density of 2 mA cm^{-2} for 60 s (a charge of 0·12 C cm^{-2}) in the 0·1M KCl solution to form AgCl on the surface. During reduction at −0·1 mA cm^{-2}, a potential plateau was observed at +0·048 V(SCE) before the potential dropped to −1·4 V(SCE), the potential for water reduction on bare Ag at the current density employed. The duration of the plateau was 1220 s, which represents a charge of 0·122 C cm^{-2}, in good agreement with the charge passed during generation of the AgCl. Similar correspondence was observed for a range of AgCl generation charges, indicating that the formation and reduction processes are equally current efficient and likely close to 100% current efficient. Because the thickness of generated AgCl layer also scales linearly with generation charge, the reduction charge can be used as a measure of the thickness of AgCl layer. A reduction charge of 1 C cm^{-2} is equivalent to an average AgCl thickness of 2·68 μm, assuming theoretical density.

ASTM B825 recommends deaerated 0·1M KCl solution for the coulometric reduction method.[43] However, this solution can alter the nature of the film formed on the Ag surface, making identification of the film impossible. Figure 3 shows the reduction curves for different films on Ag samples. Curve 1 is the reduction curve for a sample on which both AgCl and Ag_2O were formed, curve 2 is for a sample on which only AgCl was formed and curve 3 is for a sample on which only Ag_2O was formed. All samples were reduced in 0·1M KCl solution. The three samples exhibit the exact same reduction potential, which is the characteristic potential for silver chloride reduction. This observation indicates that the silver oxide films were converted to silver chloride by exposure to the chloride solution and that the different products cannot be distinguished by coulometric reduction in chloride solution as described by ASTM B825. Figure 4 shows the reduction curves for different samples in 0·1M Na_2SO_4 solution at pH 10. Both silver chloride and silver oxide are stable in this solution. Curve 1 is the reduction for silver oxide, curve 2 is the reduction for silver chloride and curve 3 is the reduction for the mixture of silver oxide and silver chloride. The characteristic potentials for oxide and chloride are clearly distinguished by a difference of ∼100 mV. Note that the value for chloride reduction in the sulphate solution is different than in the 0·1M chloride solution, as expected. The sample with a mixture of oxide and chloride exhibited two clear plateaus, one at each characteristic potential. In some cases, a shoulder at the AgCl reduction potential was observed even in the sulphate solution. This result was attributed to contamination of the solution by the SCE, and subsequently an MSE electrode was used for reduction in the sulphate solution.

The reduction of silver oxide was investigated by first performing cyclic voltammetric (CV) scanning in 0·1M NaOH. The potential was scanned at a rate of 25 mV s^{-1}

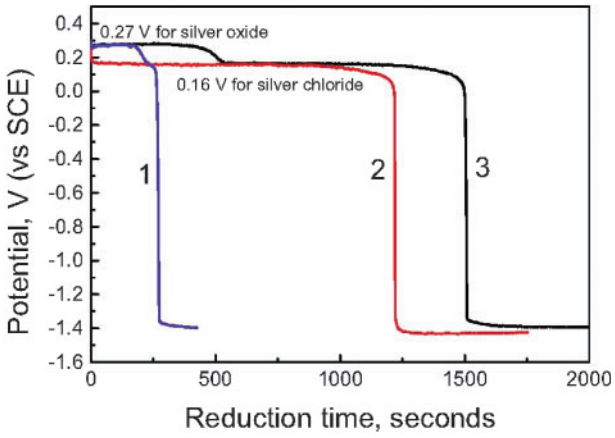

4 Potential versus time for coulometric reduction ($-0{\cdot}1$ mA cm^{-2}) of the oxidised silver samples in deaerated 0·1M Na_2SO_4 (pH=10) solution. Before reduction, silver chloride was formed by coulometric oxidation at 2 mA for 60 s in 0·1M KCl solution (Curves 2 and 3), and silver oxide was formed by potentiodynamic scanning from −1680 to 900 mV with a rate of 100 mV s^{-1} in 1M NaOH solution (Curves 1 and 3)

over the range of −1·68–0·9 V(SCE). Four peaks are identified in the CV curve shown in Fig. 5. Anodic peaks A1 and A2 at around 0·405 and 0·75 V(SCE) correspond to the formation of Ag_2O and AgO respectively. The cathodic peaks C1 and C2 correspond to the reduction of AgO and Ag_2O respectively. Samples were polarised in 0·1M NaOH at 0·405 V(SCE) for 50–1000 s to form Ag_2O and then subjected to galvanostatic reduction in deaerated 0·1M Na_2SO_4 at pH 10. The pretreatment was performed potentiostatically to prevent AgO formation; thus, the charge was not controlled. As shown in Fig. 6, the generation charge did not increase monotonically for different experiments with increasing polarisation time in the NaOH solution, indicating variability in the efficiency of the oxidation process (the generation charge was calculated from the integration of the current–time curve). Nonetheless, the reduction charge increased with increasing polarisation time in the NaOH solution and generally increased with increasing generation charge. For the shorter generation times, the reduction charge was less

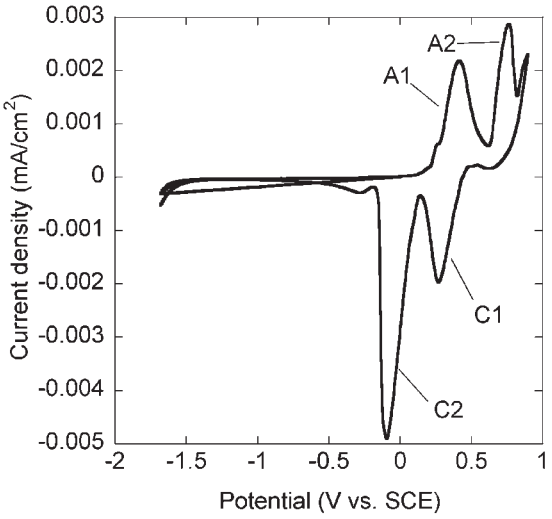

5 Cyclic voltammetric curve for bare Ag in aerated 0·1M NaOH

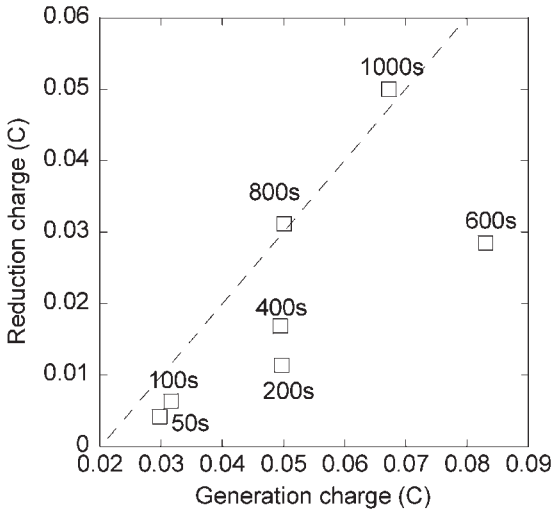

6 Reduction charge in 0·1M Na_2SO_4 at pH 10 versus potentiostatic generation charge in 0·1M NaOH at 0·405 V(SCE) for different times, which are indicated on plot

than the generation charge. This effect could be the result of another reaction besides oxide formation, so that the generation process was not 100% current efficient. Some of the Ag_2O might have dissolved during the generation process, or some amount of oxygen evolution might have occurred. Small bubbles were observed gradually to form on the sample surface during the experiment process, and bigger bubbles emerged on the edge between the o-ring and the sample later in the experiment.

Effect of UV radiation on Ag corrosion

Bare Ag samples polished to 600 grit were exposed in the chamber with about 40 ppm O_3 and 90% RH, at a gas flowrate of 892 cm^3 min^{-1}. Figure 7*a* is a picture of a sample exposed in a dark chamber without any light source for 48 h. The surface remained highly reflective after exposure indicating little corrosion product layer formation. Figure 7*b* is an image of a sample exposed to the same environment, but with UV irradiation, for only 22 h. A layer of dark corrosion product is evident on the surface. It is clear that exposure to UV radiation and ozone generates much more corrosion product than exposure to ozone alone. The SEM images in Fig. 8*a* and *b* also reflect the difference in product layer extent. The silver sample surface exposed to UV radiation was covered by a thick layer of corrosion products, whereas the sample without UV radiation had a smooth surface. It is also clear from Fig. 8*b* that the corrosion layer on silver surface is not uniform. Energy dispersive spectroscopy analysis indicated the presence of high oxygen

a in dark for 48 h; *b* under UV light for 22 h

7 Optical images of Ag sample surfaces after exposure in 40 ppm O_3 and 90% RH

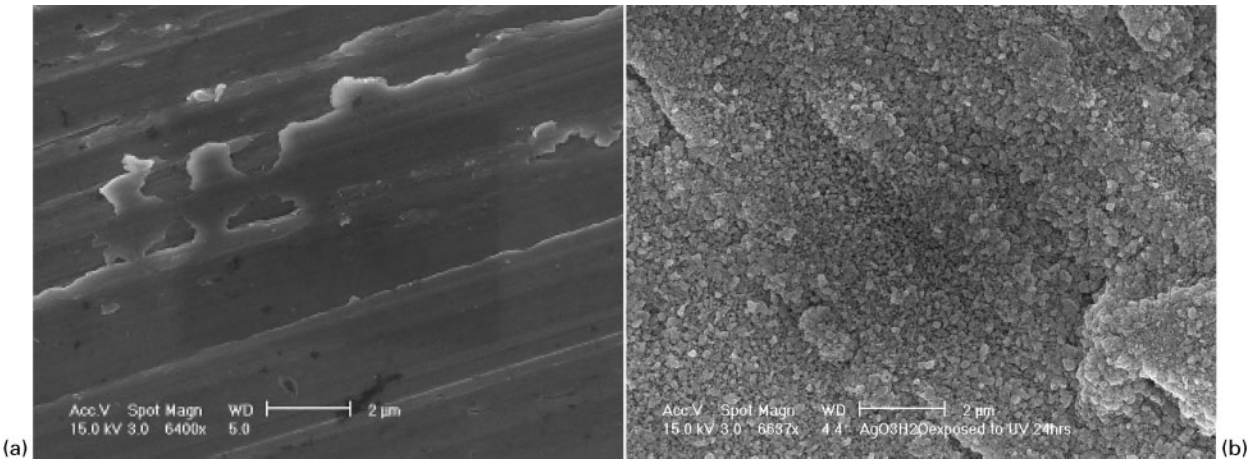

a without any light source for 48 h; *b* under UV light for 22 h

8 Images (SEM) of Ag sample surfaces after exposure in 40 ppm O_3 and 90% RH

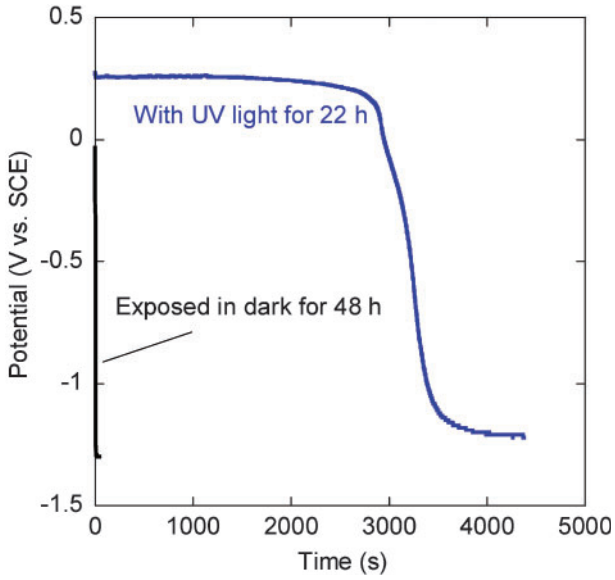

9 Coulometric reduction curve of bare Ag sample exposed in 40 ppm O_3, 90% RH, with and without UV radiation

content on the samples exposed with UV radiation and the absence of oxygen content on the samples exposed without UV radiation, as shown in Table 1 (The absolute values in Tables 1 and 2 are strongly influenced by the depth from which X-rays can be emitted during SEM examination which can be much larger than the film thickness. As such, the importance of the values is in the relative changes of the weight percentages.)

The coulometric reduction method was used to analyse the amount of corrosion product generated on the sample surfaces during the exposure. Figure 9 exhibits the reduction curves in deaerated 0·1M Na_2SO_4 at pH 10 for samples from both atmospheric environments. As shown previously, the reduction potentials for AgCl and Ag_2O in this solution are about 0·16 and 0·27 V(SCE) respectively. There was no chloride in this exposure, and the plateau potential for the black material generated on in the presence of UV light was ~0·27 V(SCE), suggesting that the product layer was Ag_2O. This interpretation is further supported by EDS analysis that found oxygen and Ag peaks dominating. The reduction current density was −0·1 mA cm^{-2}, and the area was 1 cm^2, so the 3300 s reduction time reflects a charge of 0·33 C cm^{-2}. The sample exposed in the dark exhibited a reduction curve with essentially no charge passed; the potential dropped immediately to the potential at which hydrogen evolves on bare Ag at this current density. This result is in agreement with the observations of the surface that no visible corrosion was observed.

Table 1 Energy dispersive spectroscopy profile of bare Ag exposed in 40 ppm O_3, 90% RH with and without UV radiation

	C	O	Ag	Total
With UV	3·38	8·66	87·96	100
Without UV	2·86	…	97·14	100

Effect of ozone on Ag corrosion

The effect of UV could be due to UV radiation alone or to the combined effect of UV and ozone. Furthermore, it is of interest to know if reactive species could be generated from interaction of the UV lamp with O_2 in the exposure chamber to an extent that would result in significant corrosion of Ag. To investigate these issues, an Ag sample was exposed to gas flowrates of 89·2 cm^3 min^{-1} O_2 and 803 cm^3 min^{-1} N_2 with 90% RH and UV radiation for 22 h. The O_3 generator was kept off, and no detectable O_3 was found in the exhaust gas by UV-vis spectroscopy during the exposure. No visible corrosion was observed on the sample surface as shown in Fig. 10, and this was supported by the coulometric reduction curve, which exhibited an immediate potential drop to low values.

Table 2 Energy dispersive spectroscopy profile of environmentally corroded Ag sample exposed in salt spray chamber for 2 weeks*

Element	C	O	Cl	Ag	Total
wt-%	2·26	0·67	5·69	91·38	100

*This sample was initially exposed in 40 ppm O_3, 90% RH with UV radiation for 22 h

10 Picture of sample surface after exposure to $O_2+N_2+RH+UV$ for 22 h. Specific conditions: flowrates of 89·2 cm^3 min^{-1} O_2, 803 cm^3 min^{-1} N_2, 90% RH and UV radiation

A different UV lamp (UVP Pen-Ray photochemical quartz lamp) was also tested. This smaller lamp was placed inside the cell in contrast to the standard lamp that was shined through a quartz window into the cell. The quartz window will filter out radiation with wavelength <254 nm. In this set of experiments, the flowrate of oxygen was set to be 89·2 cm^3 min^{-1}, and the flowrate of nitrogen was set at 803 cm^3 min^{-1}. When the ozone generator in the flow path was turned on and Pen-Ray UV lamp was kept off, the ozone concentration was measured as 3 ppm. However, when the Pen-Ray UV lamp was turned on to illuminate the cell and the ozone generator was turned off, the ozone concentration increased to 30 ppm within 30 min. When purified air was used as the carrier gas (1 L min^{-1}) and the UVP-Ray photochemical quartz lamp was used, the ozone concentration in the cell also increased rapidly, reaching a steady state of 45 ppm. As mentioned above, no ozone concentration change was observed using the standard Jelight UV lamp located outside the cell, and rapid corrosion was not observed when the ozone generator was turned off, even with the standard UV light on and O_2 present in the cell.

Ag samples were exposed for 22 h in an environment with UV radiation, ~90% RH, and different O_3 concentrations ranging from 0·633 to 37 ppm. It should be noted that experiments at 0·633 and 1·1 ppm O_3 were conducted at a total flowrate of 892 cm^3 min^{-1} with 1 cm^3 min^{-1} O_2 flowrate, whereas experiments at 20 and 37 ppm O_3 were conducted at a total flowrate of 446 cm^3 min^{-1} with 67 cm^3 $min^{-1}O_2$ flowrate. The surfaces of all samples turned black during the exposure as a result of the formation of silver oxide as described above. Figure 11 shows that the darkness of the surface, and thus, the apparent amount of product increased with increasing ozone concentration. The SEM images in Fig. 12 show the same trend that the surface was covered by more corrosion products as ozone concentration increased.

Coulometric reduction was performed on the samples in deaerated 0·1M Na_2SO_4 solution at pH 10 to quantify the amount of corrosion products. As shown in Fig. 13, the reduction times for sample exposed to 0·633, 1·1, 20 and 37 ppm O_3 concentration were about 120, 370, 5000 and 7100 s respectively. A lower total flowrate was used at 20 and 37 ppm O_3 compared to the low ozone conditions. The reduction times at higher ozone concentration were much higher than at low ozone concentration even though the lower flowrate might be expected to decrease the corrosion rate.[16] Given the reduction current density of 10^{-4} A cm^{-2}, these times correspond to 0·012, 0·037, 0·50 and 0·71 C cm^{-2} reduction charge respectively. A reduction charge of 0·76 C cm^{-2} was measured for the front side

a 0·633 ppm O_3; *b* 1·1 ppm O_3; *c* 20 ppm O_3; *d* 37 ppm O_3

11 Images of samples after exposure to 90% RH with UV radiation and varying ozone concentration for 22 h

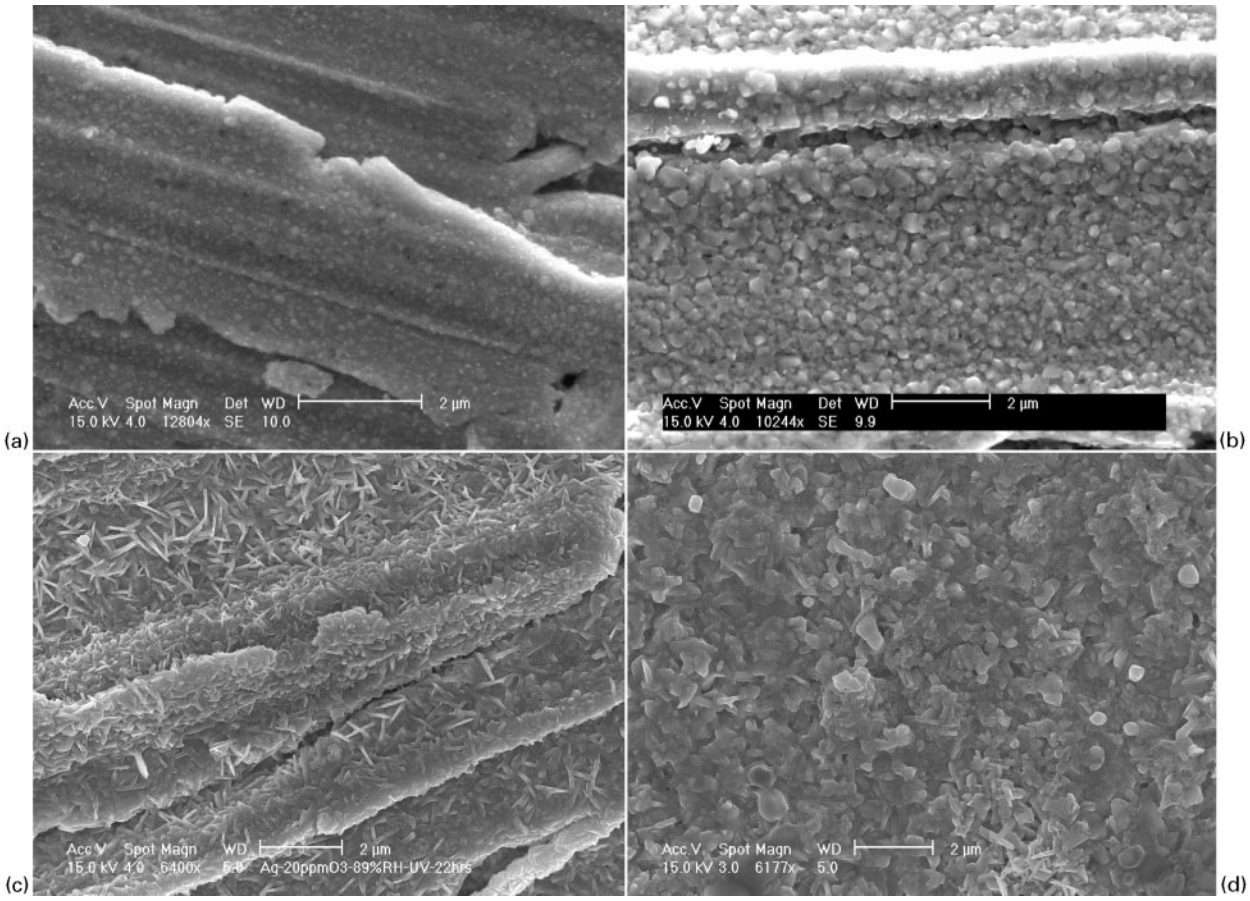

a 0·633 ppm O_3; *b* 1·1 ppm O_3; *c* 20 ppm O_3; *d* 37 ppm O_3

12 Images (SEM) of sample surfaces after exposure to 90% RH with UV radiation and varying ozone concentration for 22 h. Micron marker=2 μm

of a sample that had been exposed to the purified air and the UVP-Ray photochemical quartz lamp (O_3 concentration, 45 ppm) for 24 h, consistent with the above results. In addition, reductions in the surface of that sample that did not face the UV lamp showed virtually no silver oxide formation, demonstrating the importance of the interaction of the UV with the ozone at the metal surface.

Effect of relative humidity

The effect of RH was also examined. The O_2 flowrate was controlled below 1 cm^3 min^{-1} to generate a low concentration of ozone (0·633 ppm). The total gas flowrate was 892 cm^3 min^{-1}. Polished bare Ag pieces were exposed to an environment with UV, 0·633 ppm O_3 and RH ranging from 90 to 0% (dry condition) for 22 h. After the experiments, samples were taken out from the exposure chamber and subjected to coulometric reduction analysis in deaerated 0·1M Na_2SO_4 at pH 10. Figure 14 shows the reduction curves, and Fig. 15 shows the reduction charge as a function of RH. The reduction potential of all these samples was around -125 mV_{MSE}, which is the characteristic reduction potential for Ag_2O. Furthermore, there was a weak effect of RH on reduction time and charge; the average reduction charge increased from 0·011 to 0·014 C cm^{-2} as RH dropped from 90 to 60%, whereas the data at 0% were quite scattered but had a similar average charge as those at higher RH.

Effect of exposure time

Although atomic oxygen is extremely oxidising,[44–46] it is of interest to know the kinetics of the reaction with bare silver. In this set of experiments, bare Ag samples were exposed to environments with UV, 0·633 ppm O_3, and 90% RH for 1, 5, 10 or 22 h, 0·633 ppm O_3, 0% RH for 1 and 5 h and 1·1 ppm O_3, 90% RH for 1 and 5 h respectively. After exposure, samples were subjected to galvanostatic reduction in deaerated 0·1M Na_2SO_4 solution at pH 10. In Fig. 16, the galvanostatic reduction curves show that oxidation process on silver did not start immediately; instead, an incubation time was needed, and the incubation time was different for the different conditions. The reduction charges calculated from the reduction times are shown in Fig. 17*a*. No measurable reduction charge was found after 1 h for 0·633 ppm O_3 in both dry and wet conditions, which means no corrosion product was generated during exposure. The reduction charge curve for 0·633 ppm O_3, 90% RH exhibits a sigmoidal shape, increasing rapidly after the incubation time and slowing as the oxide thickened, possibly because of diffusion limitation. A qualitatively similar behaviour was observed for the 45 ppm ozone condition as seen in Fig. 17*b*, albeit with much larger charge densities due to the higher ozone concentration. These results are consistent with other researchers who studied the reaction rate of atomic oxygen with bare silver.[47]

Salt spray testing of Ag with environmentally generated Ag_2O

An Ag sample was exposed to 40 ppm O_3, 90% RH and UV radiation for 22 h. The sample was then placed in an

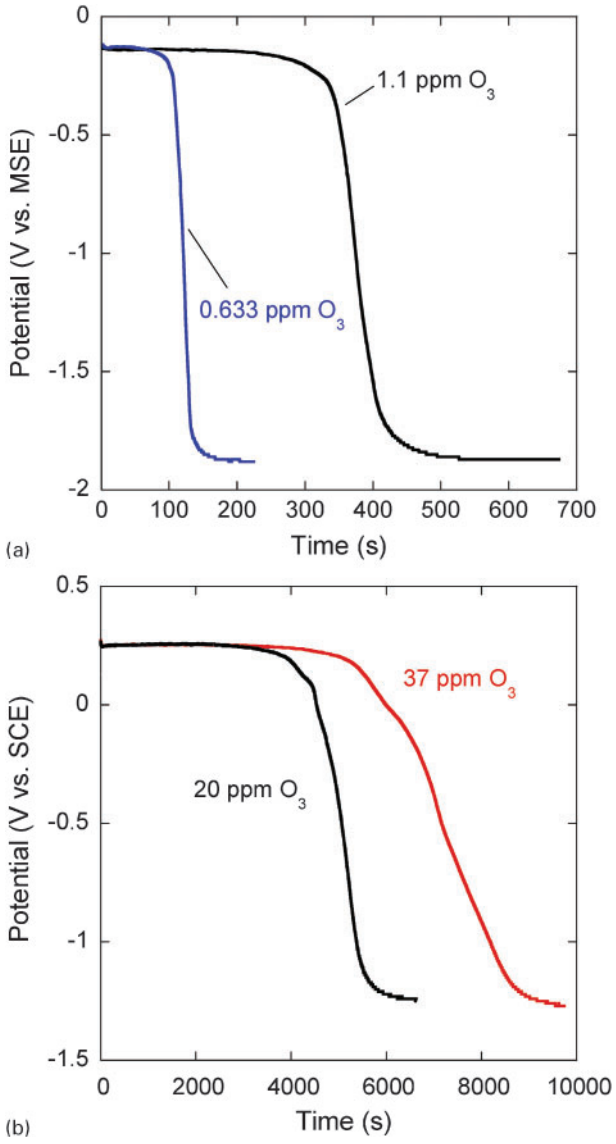

a 0·633 and 1·1 ppm O_3, 90% RH; *b* 20 and 37 ppm O_3, 90% RH

13 Coulometric reduction curves for bare Ag after exposure to UV radiation, ~90% RH, and different levels of ozone concentrations for 22 h

ASTM B117 salt spray chamber for 2 weeks. After salt spray exposure, the sample was ultrasonically rinsed with DI water, and then subjected to the galvanostatic reduction in deaerated 0·1M Na_2SO_4 solution at pH 10.

After the initial exposure to ozone+UV, the sample surface was covered with a black silver oxide product layer as described previously (Fig. 18*a*). After the salt spray exposure, the sample surface was white (Fig. 18*b*). An SEM image of the white corrosion product on the surface after the salt spray test is exhibited in Fig. 18*c*. Voluminous corrosion products are observed. The composition of the entire area of corrosion products as determined by EDS is shown in Table 2. Comparing this composition to Table 1, it is clear that the O content decreased while the Cl content increased as a result of the salt spray test. It is likely that the silver oxide formed in the UV chamber is converted to chloride in the salt spray chamber. This result is expected because silver chloride is thermodynamically more stable than silver oxide (also shown from the reduction potential as

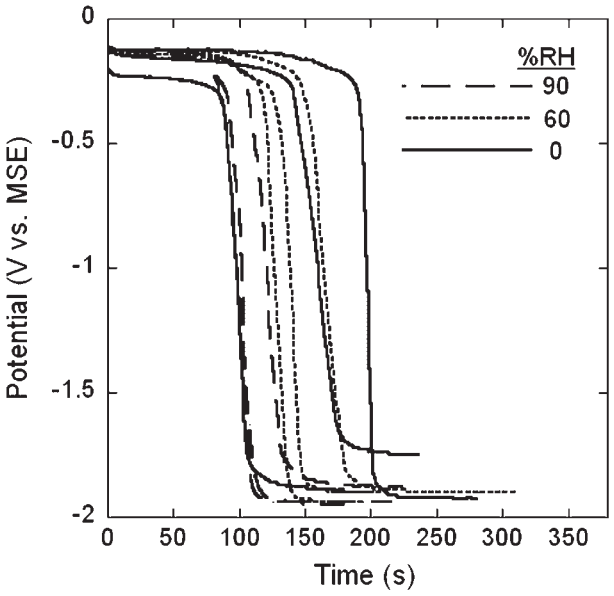

14 Coulometric reduction curves for bare Ag sample exposed to UV, 0·633 ppm O_3 and from 90 to 0% (dry condition) for 22 h.

silver chloride has a lower reduction potential than silver oxide, which is around 250 mV(SCE)). Figure 19 shows the reduction curve for this sample. The reduction charge is calculated to be 0·038 C cm^{-2}, which is smaller than that of a sample after the same exposure but before salt spray test (0·6 C cm^{-2}). It is possible that ultrasonic cleaning removed some corrosion product from sample surface. The potential, ~+100 mV(SCE), is lower than that expected for either silver oxide or chloride when reduced in the pH 10 Na_2SO_4 solution. A freshly polished bare silver sample remained shiny after 2 weeks exposure to the salt spray environment.

Discussion

The first part of this investigation focused on the refinement of a coulometric reduction method, which

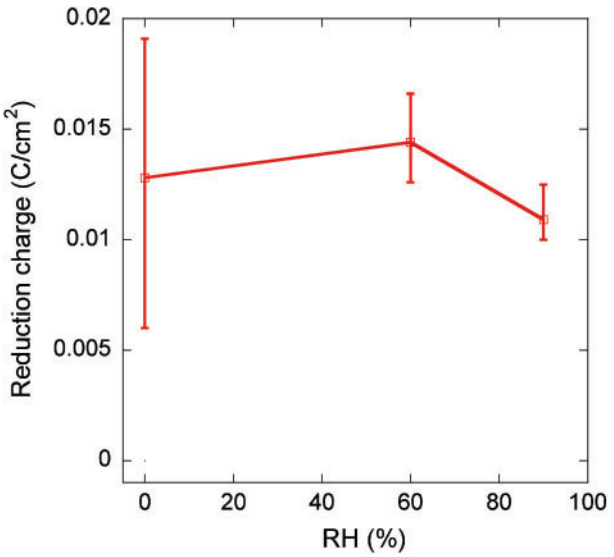

15 Reduction charge for bare Ag sample exposed to UV, 0·633 ppm O_3 and RH ranging from 90 to 0% (dry condition) for 22 h. Bars represent scatter of three samples for each condition

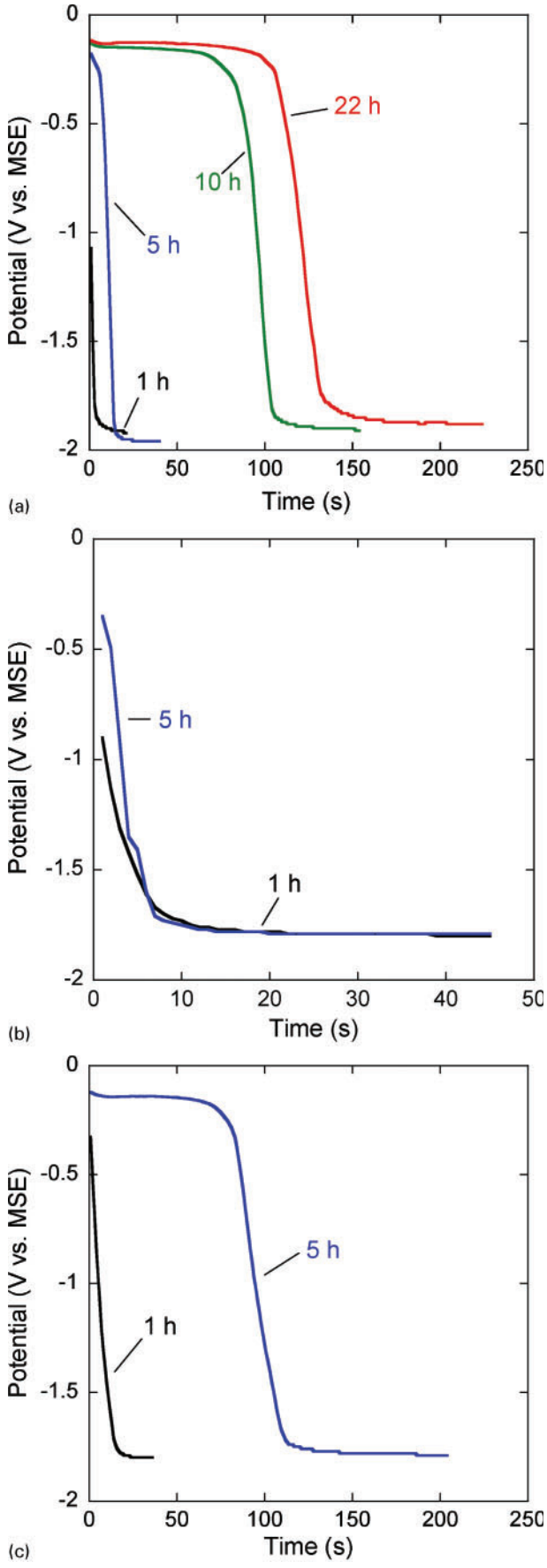

a 0·633 ppm O_3, 90% RH for 1, 5, 10 and 22 h; *b* 0·633 ppm O_3, 0% RH for 1 and 5 h; *c* 1·1 ppm O_3, 90% RH for 1 and 5 h

16 Coulometric reduction curves for Ag exposed to UV

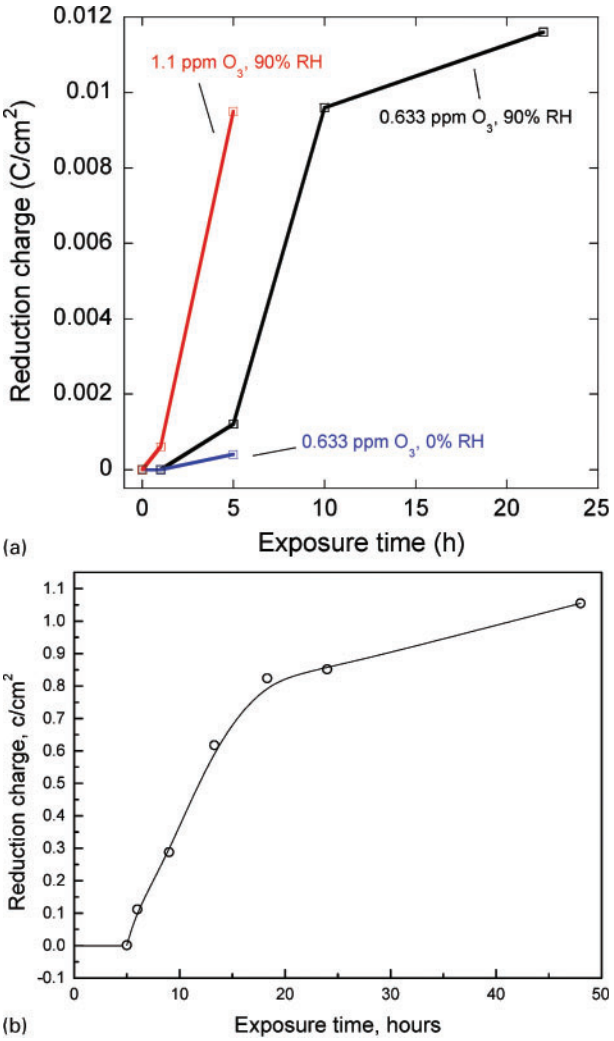

a after exposure to UV in 0·633 ppm O_3, 90% RH for 1, 5, 10 and 22 h, 0·633 ppm O_3, 0% RH for 1 and 5 h and 1·1 ppm O_3, 90% RH for 1 and 5 h; *b* after exposure to UV in 45 ppm O_3 and 90 % RH

17 Reduction charge versus time for bare Ag

has been used historically to assess corrosion products formed on silver and copper.[15,23,43,48,49] It was shown that silver oxide rapidly transforms to a chloride product that exhibits the reduction potential characteristic of silver chloride when exposed to the KCl reduction solution. This transformation was avoided using 0·1M Na_2SO_4 solution (pH 10), allowing oxide and chloride corrosion products to be distinguished by the reduction potential. The corrosion product formed on silver by the experiments that involved exposure to gaseous environments containing water vapour and ozone, with UV radiation, did not generate chloride product. The revised method was also useful for the sample exposed to a salt spray chamber after a previous exposure in the $RH+O_3+UV$ environment. Another paper will report the results of experiments on Ag samples with nanosized NaCl particles deposited on the surface before exposure.

The focus of most of this work was on the combined effects of ozone, RH and UV. Samples exposed to the same conditions of RH and ozone exhibited vastly different corrosion behaviour depending on the irradiation condition. Samples exposed in the dark were

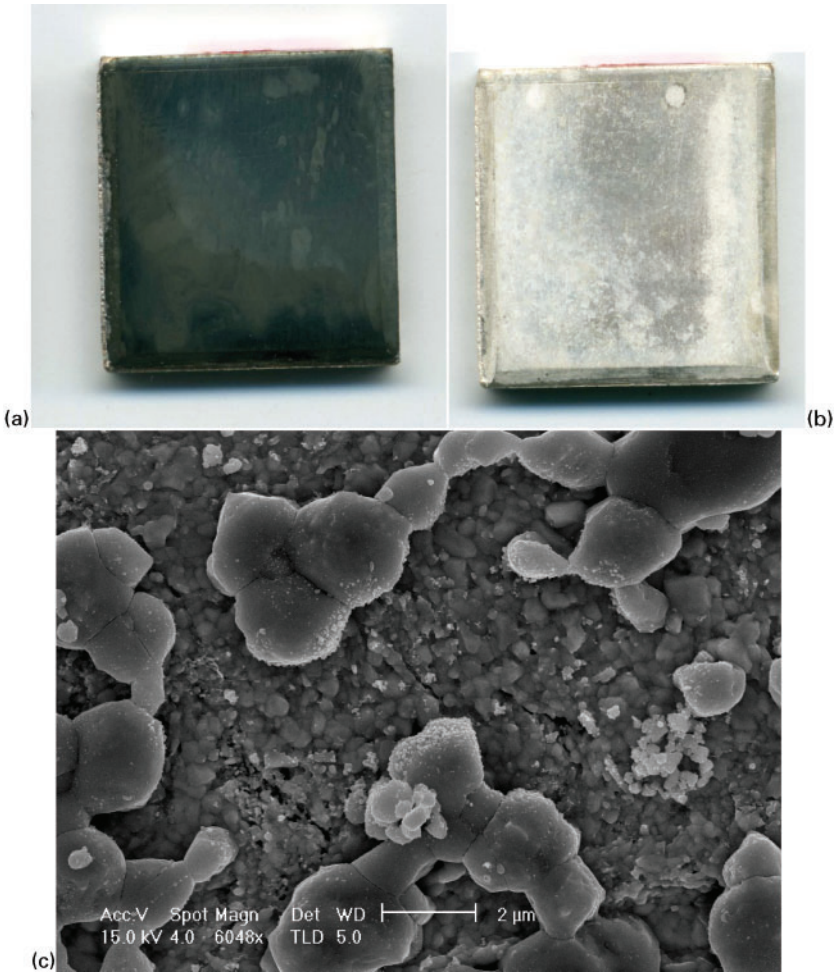

a after exposure in O_3, RH and UV; *b* after exposure in salt spray chamber for 2 weeks; *c* SEM image after salt spray exposure

18 Images of Ag sample

essentially uncorroded, whereas the samples exposed in the presence of 254 nm UV radiation exhibited fast corrosion as evidenced by the nature of the surface and the reduction charge. In analogous experiments with an exposure of samples to 90% RH and UV radiation, but no ozone, no measurable corrosion was observed during the standard 22 h exposure period. Hence, it was shown that fast silver corrosion requires the combined presence of UV and ozone. The extent of corrosion increased with increasing ozone concentration.

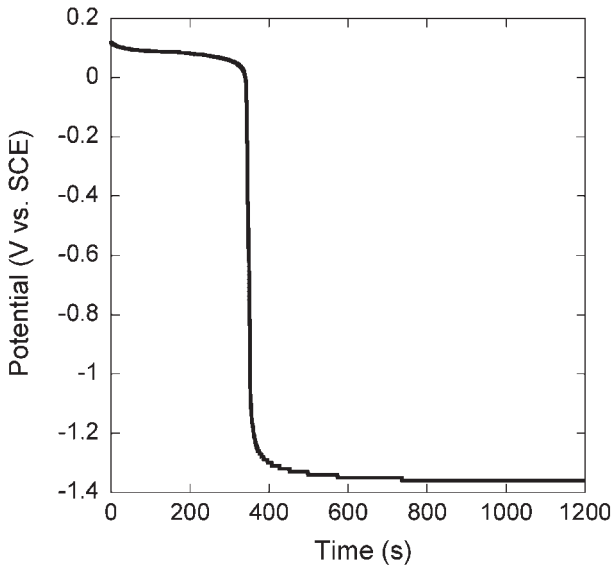

19 Reduction curve for sample after exposure in salt spray chamber for 2 weeks. Ag sample was first exposed to 40 ppm O_3, 90% RH and UV radiation for 22 h

These exposure results can be explained by the interaction among UV radiation, O_3 and bare silver. It is known that UV light of wavelength <310 nm is able to photodecompose ozone to form molecular oxygen and atomic oxygen as shown in reaction (1),[5,41,42] so the role of each of these species should be considered. Molecular oxygen cannot oxidise silver at ambient temperature, and the interaction with silver is mainly limited to adsorption.[46,50,51] The effects of ozone are discussed below. However, atomic oxygen is a highly oxidising species and can react with many materials.[44–46] It has been reported that silver changes from shiny metallic to grey after exposure in an atomic oxygen rich environment, and the corrosion product was identified as Ag_2O.[52] The reactions between atomic oxygen and silver are expected to be

$$2Ag + O = Ag_2O \quad (3)$$

$$Ag_2O + O = 2AgO \quad (4)$$

Hence, bare silver will react with atomic oxygen generated from photodecomposed ozone to form silver oxide. Because atomic oxygen is not generated in the absence of UV light and ozone alone does not react quickly with bare silver, no measurable corrosion product is generated in the dark during the exposure time.

The absence of significant corrosion for the sample exposed to an environment containing oxygen in the presence of UV radiation can be explained by the wavelength of the light used to irradiate the sample in the cell. The Jelight UV lamp was not able to break down oxygen to form molecular oxygen according to reaction (2). Radiation of wavelength 242 nm or less is required for this reaction, and the lowest wavelength emitted by the Jelight lamp was 254 nm. Another UV source, the Pen-Ray lamp, when placed inside the cell, was able to create ozone, even with the ozone generator turned off, when oxygen was present in the gas stream, as evidenced by the measurement of ozone in the exit gas. It is likely that the atomic oxygen was the species responsible for the accelerated corrosion attack under these circumstances. However, the experimental system had no means to assess atomic oxygen concentration, only ozone. The ozone generated and sensed is formed by the recombination of an oxygen atom with an oxygen molecule according to

$$O + O_2 \rightarrow O_3 \tag{5}$$

The lack of an effect of RH on the corrosion process for bare Ag at this ozone concentration is in contrast to most cases of atmospheric corrosion where the corrosion rate decreases as RH decreases.[9–11] A possible explanation is as follows. In common atmospheric corrosion, as RH decreases, there is less water to dissolve the ionised metal, and also, less pollutant particles will be adsorbed on metal surface at lower RH. Hence, the corrosion rate usually drops when RH decreases.[9–11] When the RH decreases below the critical RH associated with deliquescence of any salt contamination on the surface, corrosion decreases to very low values, as there is very little water on the surface. For the clean surfaces studied here, the critical humidity is close to 100% RH. Below the critical RH, the presence of O_3 alone does not result in fast silver corrosion. However, UV radiation and ozone interact to form atomic oxygen[44–46] that, even at high RH, reacts with silver in a process similar to the dry corrosion process that occurs at 0% RH. Under dry conditions, the corrosion process of atomic oxygen on bare silver seems to start with chemisorption of atomic oxygen on the silver surface.[51,53–55] Atomic oxygen will adsorb at vacant sites to eventually form a monolayer. The surface coverage of atomic oxygen was found to be critical in the oxidation process of Ag.[46,56] The formation of chemisorbed oxygen is thermodynamically favoured over oxide formation at low surface coverage of adsorbed atomic oxygen, while the formation of oxide is more favoured at sufficient surface coverage.[57,58] In the presence of humidity, a layer of thin adsorbed water will be formed. In this case, atomic oxygen will react with water to form hydroxyl (OH) radical, as shown in reaction (6).[59,60] OH radical can also react with Ag to form Ag_2O and H_2O according to reaction (7). Similar to atomic oxygen, chemisorption of OH radical has also been observed on a silver surface,[59–62] and it is likely that reaction (7) starts with chemisorption of OH radical. The calculated adsorption energy of OH radical (76·2 kcal mol^{-1}) and atomic oxygen (87·1 kcal mol^{-1}) are close.[63] Hence, the rate of chemisorption in both dry and wet conditions could be similar. Moreover, as the silver oxide layer forms, it will act as a transport barrier for reactive species. As a result of the similar initial chemisorption in both dry and wet conditions and formation of transport barrier, the corrosion rate of bare silver in an environment of UV light, RH and ozone is not sensitive to the change of RH.

$$O + H_2O = 2OH \tag{6}$$

$$Ag + 2OH = Ag_2O + H_2O \tag{7}$$

Samples exposed for different times to an environment containing RH, ozone and UV radiation showed that the reaction did not begin immediately. This incubation time could be related to the chemisorption process of OH radical at wet condition or atomic oxygen at dry condition on the bare silver surface. It is clear from Fig. 16*a* and *b* that the incubation times for 0·633 ppm O_3 at both 0 and 90% RH are similar, which is between 1 and 5 h. The kinetics of the chemisorption process could be similar for atomic oxygen and OH radical. It was observed that there has to be sufficient surface coverage of adsorbed atomic oxygen to initiate the oxidation process.[57] Hence, it is possible that the oxidation of silver by OH radical also begins with the initial chemisorption process and will not start until the surface coverage reaches certain level. The increase in the amount of attack with increasing O_3 concentration is expected because as O_3 concentration increases, the amount of atomic oxygen that is generated by UV radiation will also increase. As a result, the degree of corrosion increased correspondingly.

It should also be mentioned that the reduction potential for 0·633 ppm O_3, 90% RH after 5 h exposure is about -200 mV_{MSE}, which is about 70 mV lower than that after 10 or 22 h. A similar low potential was also observed for 0·633 ppm O_3, 0% RH after 5 h exposure and 1·1 ppm O_3, 90% RH after 1 h exposure, as they both exhibit low reduction charge. It is possible that the chemisorbed layers exist on the surface (the reduction time for a monolayer is only $\sim$4·5 s, assuming a close packed silver plane), whereas a silver oxide layer forms at longer exposure times. It can also be seen that a higher ozone concentration (1·1 ppm O_3) results in faster formation of a chemisorbed atomic oxygen layer (1 h) and faster corrosion (0·0094 C cm^{-2} after 5 h exposure), which could be due to a higher concentration of atomic oxygen generated during exposure.

Conclusions

The reaction of Ag in environments containing ozone, humidity and UV radiation was studied. The following conclusions can be drawn.

1. The presence of both ozone and UV radiation are necessary for rapid corrosion, because the photodissociation of ozone generates reactive atomic oxygen, which reacts with Ag rapidly to form Ag_2O.

2. In the presence of UV radiation, corrosion on the Ag surface tends to become more severe as the ozone concentration in the environment increases.

3. The corrosion reaction on bare silver was barely affected by the RH in the environment, which is contrary to common atmospheric corrosion experience. Atomic oxygen reacts directly with Ag under dry conditions but, in the presence of humidity, probably reacts with water to form OH radical, which then reacts with the Ag. The reactions of both O and OH with bare silver start with the chemisorption process, which is similar for these two species. The generated corrosion layer then acts as a transport barrier in a similar way for both reactive species, which controls the corrosion kinetics.

4. An incubation time is needed for initiation of Ag corrosion under these conditions. This incubation time is associated with the chemisorption of atomic oxygen or OH radical, which is the initial process before the start of oxidation process.

5. A modification of the coulometric reduction technique, substituting pH 10 sulphate solution for chloride solution, prevented the transformation of silver oxide corrosion product to chloride in the reduction solution.

Acknowledgements

This work was supported by contracts from D. Dunmire at the US Office of the Secretary of Defense, through Mandaree Enterprise Corp. The guidance and input of W. Abbott and R. Kinzie are greatly appreciated.

References

1. 'Standard practice for operating salt spray (fog) testing apparatus', in 'Annual book of ASTM standards', B117-97, Vol. 3.02, ASTM, Philadelphia, PA, 2000.
2. B. J. Finlayson-Pitts: *Chem. Rev.*, 2003, **103**, 4801–4822.
3. K. W. Oum, M. J. Lakin, D. O. DeHaan, T. Brauers and B. J. Finlayson-Pitts: *Science*, 1998, **279**, 74–77.
4. X. Yu and J. R. Barker: *J. Phys. Chem. A*, 2003, **107A**, 1313–1324.
5. E. M. Knipping, M. J. Lakin, K. L. Foster, P. Jungwirth, D. J. Tobias, R. B. Gerber, D. Dabdub and B. J. Finlayson-Pitts: *Science*, 2000, **288**, 301–306.
6. A. Laskin, H. Wang, W. H. Robertson, J. P. Cowin, M. J. Ezell and B. J. Finlayson-Pitts: *J. Phys. Chem. A*, 2006, **110A**, 10619–10627.
7. J. L. Thomas, A. Jimenez-Aranda, B. J. Finlayson-Pitts and D. Dabdub: *J. Phys. Chem. A*, 2006, **110A**, 1859–1867.
8. G. E. Shaw: *J. Geophys. Res. Atmos.*, 1991, **96**, 22369–22372.
9. H. Bennett, R. Peck, D. Burge and J. Bennett: *J. Appl. Phys.*, 1969, **40**, 3351–3360.
10. H. Kim: *Mater. Corros.*, 2003, **54**, 243–250.
11. M. Forslund, J. Majoros and C. Leygraf: *J. Electrochem. Soc.*, 1997, **144**, 2637–2642.
12. D. Rice, P. Peterson, E. Rigby, P. Phipps, R. Cappell and R. Tremoureux: *J. Electrochem. Soc.*, 1981, **128**, 275–284.
13. T. Graedel: *J. Electrochem. Soc.*, 1992, **139**, 1963–1970.
14. M. Watanabe, A. Hokazono, T. Handa, T. Ichino and N. Kuwaki: *Corros. Sci.*, 2006, **48**, 3759–3766.
15. Y. Fukuda, T. Fukushima, A. Sulaiman, I. Musalam, L. Yap, L. Chotimongkol, S. Judabong, A. Potjanart, O. Keowkangwal, K. Yoshihara and M. Tosa: *J. Electrochem. Soc.*, 1991, **138**, 1238–1243.
16. L. Volpe and P. Peterson: 'Mass-transport limitations in atmospheric corrosion', Proc. 1st Int. Symp. on 'Corrosion of electronic materials and devices', Seattle, WA, USA, 1991, Electrochemical Society, 22.
17. L. Volpe and P. Peterson: *Corros. Sci.*, 1989, **29**, 1179–1196.
18. M. Reid, J. Punch, C. Ryan, J. Franey, G. Derkits, W. Reents and L. Garfias: *IEEE Trans. Compon. Packag. Technol.*, 2007, **30**, 666–672.
19. J. Elechiguerra, L. Larios-Lopez, C. Liu, D. Garcia-Gutierrez, A. Camacho-Bragado and M. Yacaman: *Chem. Mater.*, 2005, **17**, 6042–6052.
20. J. Frankey, G. Kammlott and T. Graedel: *Corros. Sci.*, 1985, **23**, 133–145.
21. W. Abbott: *IEEE Trans. Parts Hybrids Packag.*, 1974, **PHP-10**, 24–27.
22. W. Hu, Y. Liu and R. Zhu: *J. Mater. Prot.*, 2005, **38**, 36–38.
23. R. Comizzoli, J. Franey, T. Graedel, G. Kammlott, A. Miller, A. Muller, G. Pein, L. Psota-Kelty, J. Sinclair, R. Wetzel and E. Sproles: *J. Electrochem. Soc.*, 1992, **139**, 2058–2066.
24. L. Veleva, B. Valdez, G. Lopez, L. Vargas and J. Flores: *Corros. Eng. Sci. Technol.*, 2008, **43**, 149–155.
25. P. McTigue and D. Young: *Aust. J. Chem.*, 1965, **18**, 1851–1853.
26. 'Environmental health criteria 160: ultraviolet radiation'; 1994, Geneva, World Health Organization.
27. S. Fujimoto, S. Kawachi and T. Shibata: *Proc. Electrochem. Soc.*, 1998, **98**, 366–375.
28. S. Fujimoto, T. Yamada and T. Shibata: *J. Electrochem. Soc.*, 1998, **145**, 79–81.
29. S. Moussa and M. Hocking: *Corros. Sci.*, 2001, **43**, 2037–2047.
30. D. Macdonald, E. Sikora, M. Balmas and R. Alkire: *Corros. Sci.*, 1996, **38**, 97–103.
31. C. Breslin, D. Macdonald, E. Sikora and J. Sikora: *Electrochim. Acta*, 1997, **42**, 137–144.
32. E. Sikora, C. Breslin, J. Sikora and D. Macdonald: *Proc. Electrochem. Soc.*, 1995, **95**, 344–354.
33. L. Rowe: *Corrosion*, 1961, **17**, 93–94.
34. D. Macdonald and D. Heaney: *Proc. Electrochem. Soc.*, 1999, **99**, 367–376.
35. D. Macdonald and D. Heaney: *Corros. Sci.*, 2000, **42**, 1779–1799.
36. T. Burleigh and H. Gerischer: *J. Electrochem. Soc.*, 1988, **135**, 2938–2942.
37. C. Breslin and D. Macdonald: *Electrochim. Acta*, 1998, **44**, 643–651.
38. E. Thompson and T. Burleigh: *Corros. Eng. Sci. Technol.*, 2007, **42**, 237–241.
39. C. Breslin, A. Rudd and S. Farrell: *Proc. Electrochem. Soc.*, 2001, **2001**, 788–795.
40. T. Burleigh, C. Ruhe and J. Forsyth: *Corrosion*, 2003, **59**, 774–779.
41. B. Finlayson-Pitts and J. Pitts: 'Chemistry of the upper and lower atmosphere: theory, experiments, and applications'; 2000, New York, Academic Press.
42. A. Chowdhury: *Laser Chem.*, 1998, **17**, 191–203.
43. 'Standard test method for coulometric reduction of surface films on metallic test samples', in 'Annual book of ASTM standards', ASTM B825, ASTM, Philadelphia, PA, 2007.
44. G. Sjolander: *J. Geophys. Res.*, 1976, **81**, 3767–3770.
45. W. Henderson: *J. Geophys. Res.*, 1971, **76**, 3166–3167.
46. P. Dickens, R. Heckingbottom and J. Linnett: *Trans. Faraday Soc.*, 1968, **65**, 2235–2247.
47. S. Duo, M. Li, Y. Zhang and Y. Zhou: *Rare Met. Mater. Eng.*, 2006, **35**, 1057–1060.
48. S. Krumbein, B. Newell and V. Pascucci: *J. Test. Eval.*, 1989, **17**, 357–367.
49. S. Lee and R.W. Staehle: *J. Electrochem. Soc.*, 1995, **142**, 2189–2195.
50. B. Wood: *J. Phys. Chem.*, 1971, **75**, 2186–2195.
51. A. Czanderna: *J. Phys. Chem.*, 1964, **70**, 2120–2125.
52. L. Zhang, C. Yan, Q. Qu and C. Cao: *Chin. J. Mater. Res.*, 2002, **16**, 273–278.
53. A. Myerson: *J. Chem. Phys.*, 1969, **50**, 1228–1234.
54. A. Czanderna: *J. Phys. Chem.*, 1964, **68**, 2765–2771.
55. J. Torras, J. Ricart, F. Illas and J. Rubio: *Surf. Sci.*, 1993, **1993**, 57–65.
56. G. Waterhouse, G. Bowmaker and J. Metson: *Appl. Surf. Sci.*, 2001, **183**, 191–204.
57. V. Bukhtiyarov and A. Boronin: *Surf. Rev. Lett.*, 1994, **1**, 577–579.
58. C. Carlisle, T. Fujimoto, W. Sim and D. King: *Surf. Sci.*, 2000, **470**, 15–31.
59. K. Bobrov and L. Guillemot: *Surf. Sci.*, 2007, **601**, 3268–3275.
60. L. Guillemot and K. Bobrov: *Surf. Sci.*, 2007, **601**, 871–875.
61. Z. Hu and H. Nakatsuji: *Surf. Sci.*, 1999, **425**, 296–312.
62. M. Canepa, L. Mattera and N. Naducci: *Surf. Sci.*, 1997, **371**, 431–437.
63. C. Qin and J. L. Whitten: *J. Phys. Chem. B*, 2005, **109B**, 8852–8856.